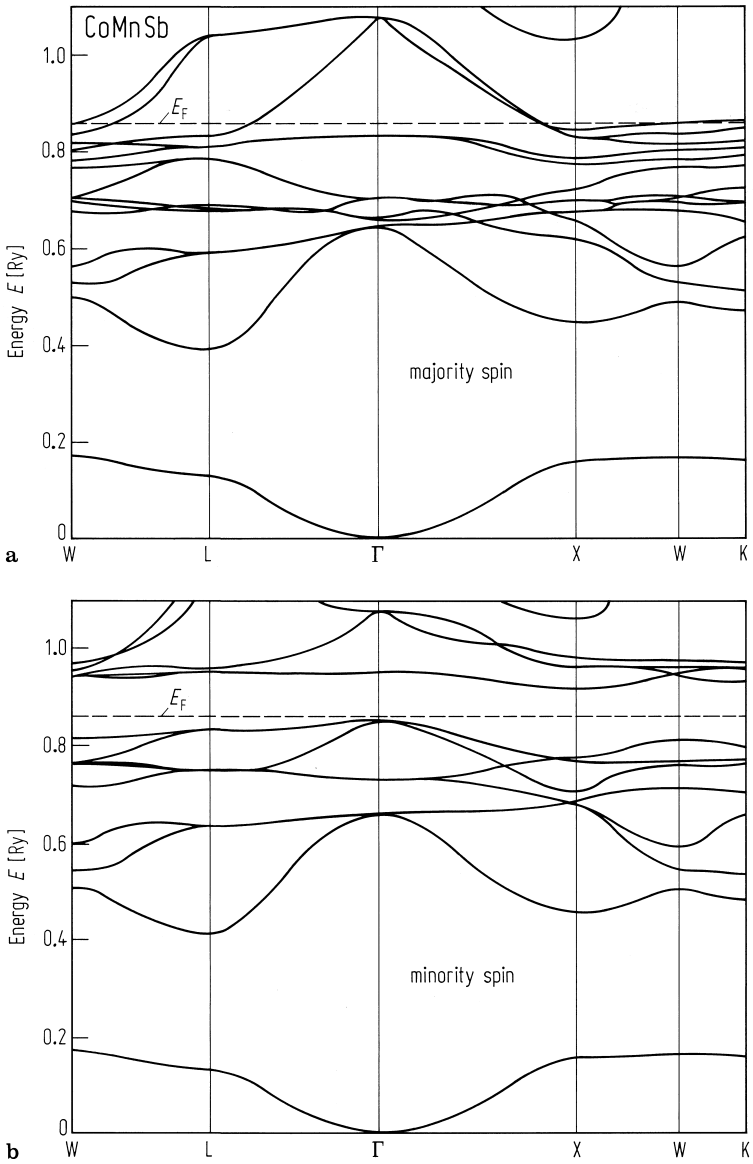

Fig. 537. (**a**) Band structure of majority-spin electrons; (**b**) or minority-spin electrons of CoMnSb [84K1].

1.5.5.9.2 Cohesion and phase transitions

The conduction electron concentration strongly influences not only the electrical and magnetic properties but also the type and degree of atomic order and phase stability. Ni_2MnGa is an example of a system which undergoes a cubic to tetragonal phase transition which is believed to be a band Jahn Teller effect. The effects of electronic band structure on the local atomic order has been calculated for Cu_2NiZn systems and the Ni_2YAl series.

Table 114. The calculated and observed equilibrium lattice constants *a* of the Heusler $L2_1$ phase Ni_2XAl (X = Ti, V, Zr, Nb, Hf and Ta) compounds, the lattice mismatch between $L2_1$ Ni_2XAl and NiAl and their formation energies E_{form}. The related data of NiAl and NiTi are also listed [92L1].

Compound	*a* (calc) [Å]	*a* (exp) [Å]	Mismatch [%]	E_{form} [mRy/atom]
Ni_2TiAl	5.87	5.872, 5.843	1.7	63.0
Ni_2VAl	5.78	6.33	1.0	47.5
Ni_2ZrAl	6.10	6.123	5.6	61.2
Ni_2NbAl	6.00	5.974, 5.970	3.9	50.9
Ni_2HfAl	6.10	6.081, 6.07	5.6	69.7
Ni_2TaAl	5.95	5.945, 5.936, 5.949	3.0	57.8
NiAl	2.88	2.887	0.0	71.0
NiTi	3.00	3.015	3.9	35.0
NiTi + NiAl				53.0

Table 115. The calculated equilibrium lattice constants *a* of the B2 phase Ni_2XAl (X = Ti, V, Zr and Nb) compounds (note that in B2-like structure, $b = a$ and $c = 2a$), the lattice mismatch between the $L2_1$ and B2 phases, the formation energies E_{form} of the B2 phase and the difference between the formation energy of the B2 and $L2_1$ phases, ΔE, [92L1].

Compound	*a* (calc) [Å]	Mismatch [%]	E_{form} [mRy/atom]	ΔE [mRy/atom]
Ni_2TiAl	2.95	0.5	54.7	8.3
Ni_2VAl	2.89	0.0	42.5	5.0
Ni_2ZrAl	3.08	1.0	43.7	17.5
Ni_2NbAl	3.02	0.7	38.5	12.4

Table 116. Values of the number of electrons per atom, n_e, corresponding to the two distinct valleys A and B (cf. Figs. 551 and 558) in the DOS of the $L2_1$ and B_2 structured Ni_2XAl (X = Ti, V, Zr, Nb, Hf and Ta) compounds [92L1].

Compound	n_e ($L2_1$)		n_e (B2)	
	A	B	A	B
Ni_2TiAl	6.00	7.07	6.00	7.99
Ni_2VAl	6.00	7.08	6.00	7.99
Ni_2ZrAl	6.00	7.06	6.00	7.98
Ni_2NbAl	6.00	7.06	6.00	8.00
Ni_2HfAl	6.00	7.07		
Ni_2TaAl	6.00	7.07		

Table 117. Comparison of number of the first, second and third nearest neighbours (NN) of Ni, X and Al atoms in the $L2_1$ and B2 structured Ni_2XAl compounds (X = Ti, V, Zr, Nb, Hf and Ta) [92L1].

Structure	Atom	First NN	Second NN	Third NN
$L2_1$	Ni	4X 4Al	6Ni	12Ni
	X	8Ni	6Al	12X
	Al	8Ni	6X	12Al
B2	Ni	4X 4Al	6Ni	12Ni
	X	8Ni	4X 2Al	4X 8Al
	Al	8Ni	4Al 2X	4Al 8X

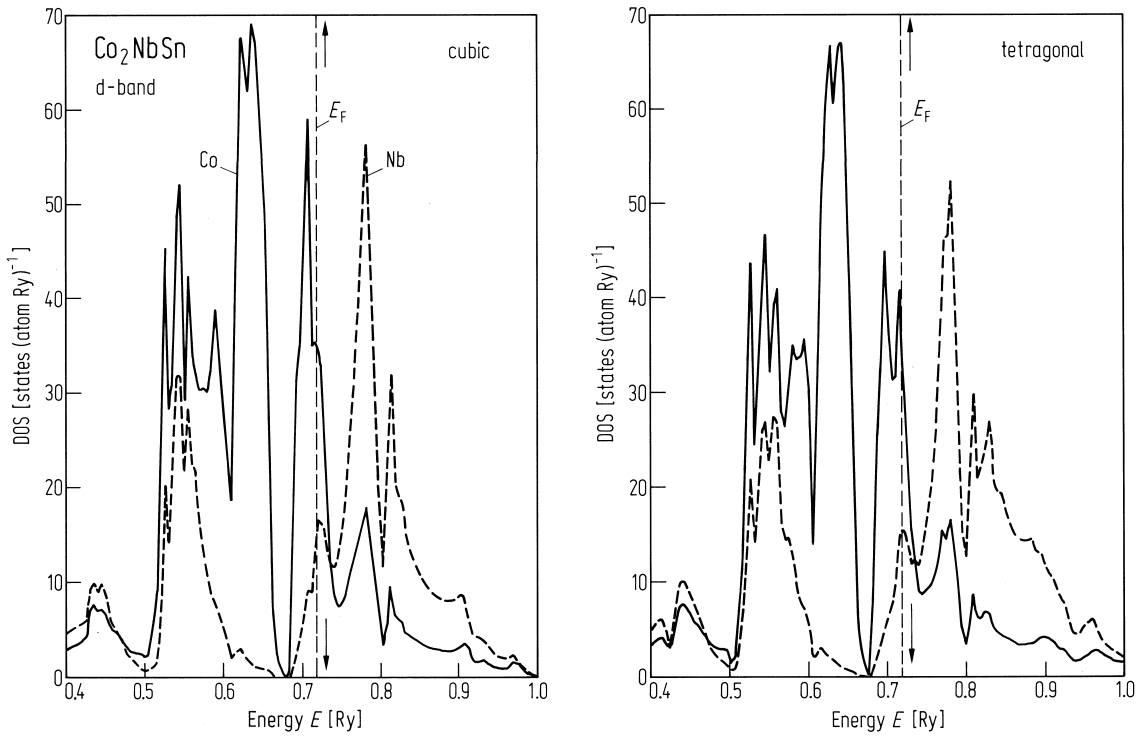

Fig. 541. DOS curves of Co_2NbSn calculated using the KKR method. The Fermi level is indicated by the vertical broken line. Arrows indicate the Fermi level of $(Co_{1-x}Ni_x)_2NbSn$ at x = 0.3. The DOS curves of d bands of Co and Nb are shown by the solid and broken curves respectively. The DOS of the cubic structure is shown on the left side and that of the tetragonal one is on the right side [89F2].

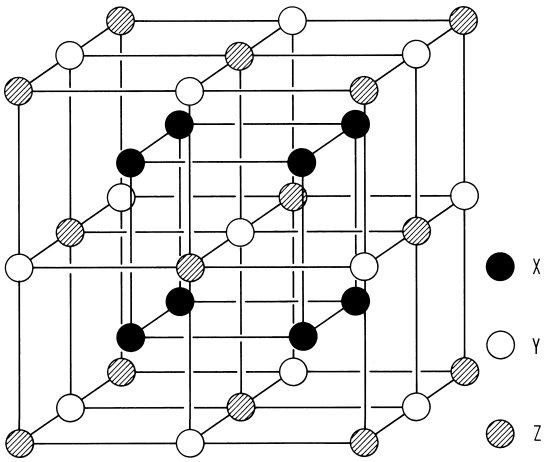

Fig. 539. Unit cell of Ni_2MnGa and Co_2NbSn (X_2YZ) in the cubic phase [89F2].

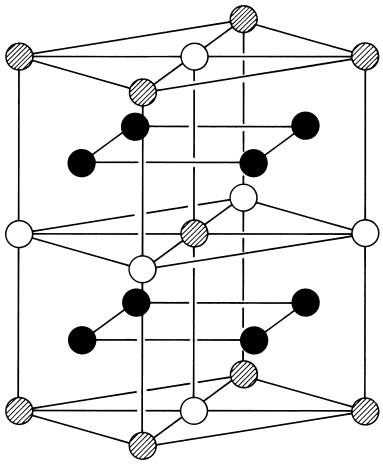

Fig. 540. The unit cells of Ni_2MnGa and Co_2NbSn in the tetragonal phase [89F2]. For symbols see Fig. 539.

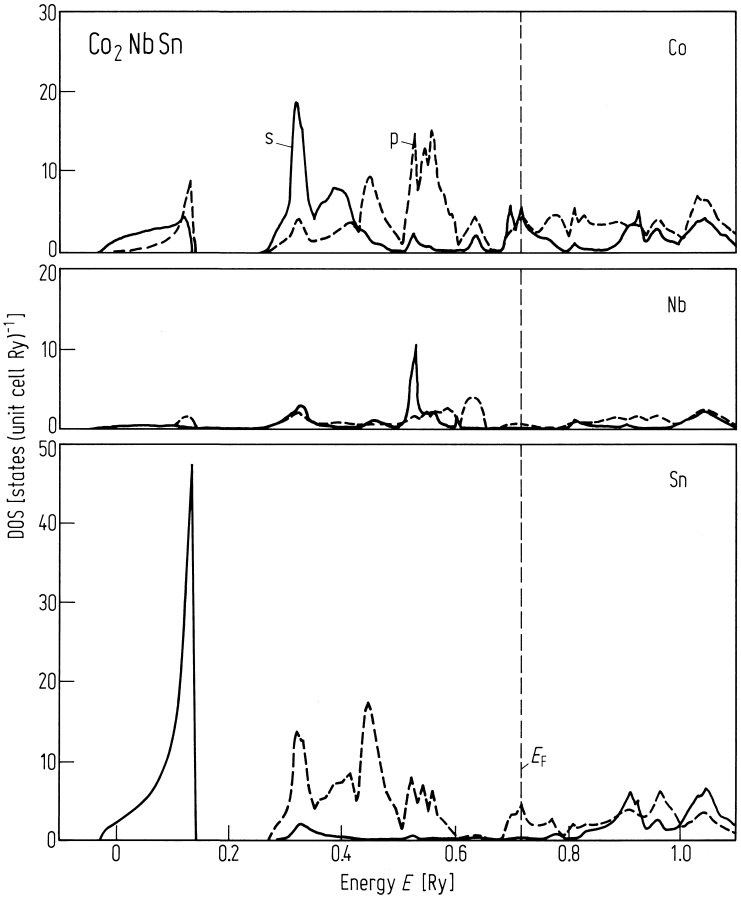

Fig. 542. DOS curves of Co_2NbSn calculated using the KKR method. The Fermi level is indicated by the vertical broken line. The DOS curves of the s and p bands of Sn, Nb and Co are shown by the solid and broken line respectively [89F2].

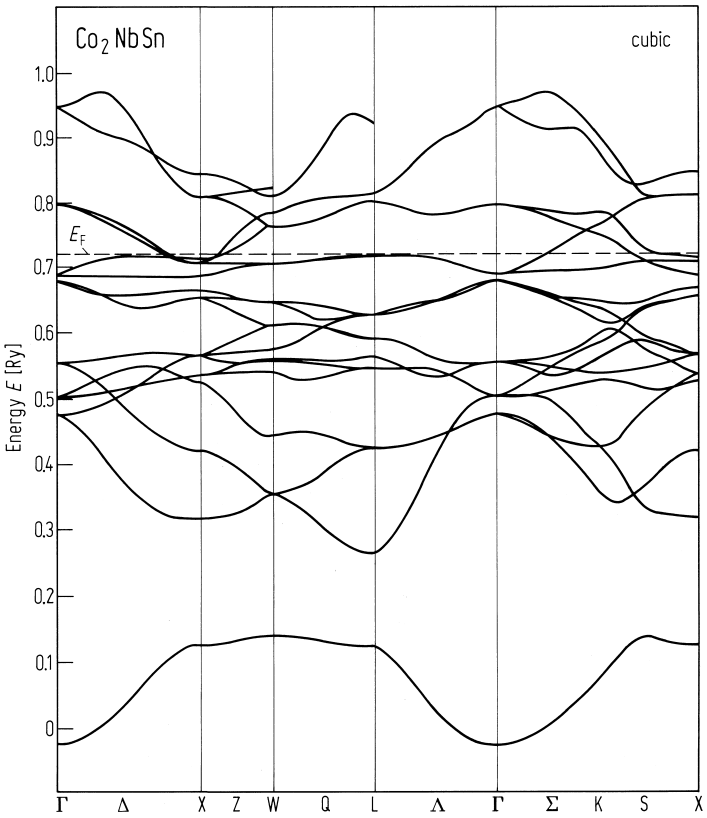

Fig. 543. $E(k)$ curves of paramagnetic Co_2NbSn, cubic structure. The Fermi level is indicated by the dashed line [89F2].

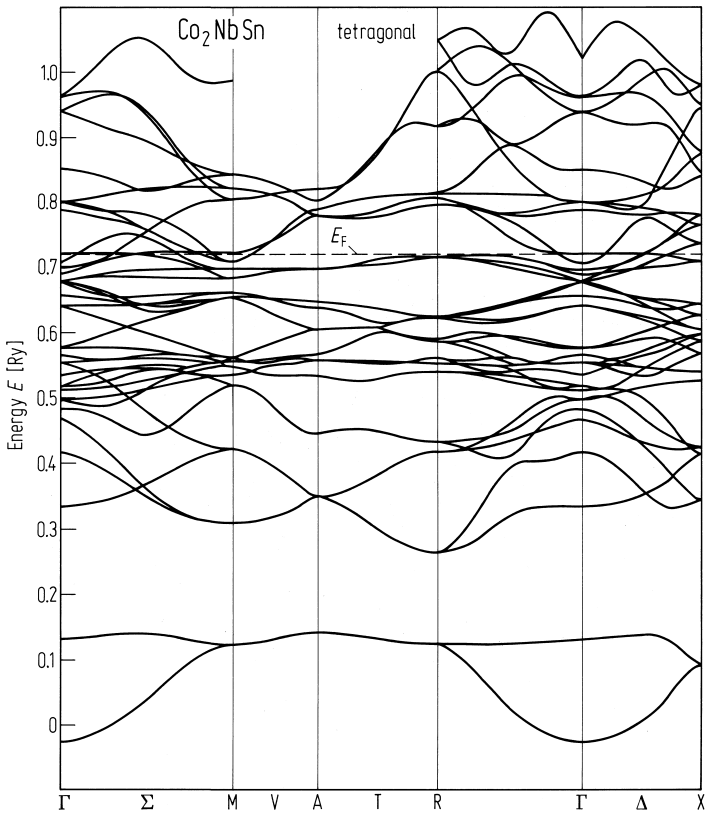

Fig. 544. $E(k)$ curves of paramagnetic Co_2NbSn, tetragonal structure. The Fermi level is indicated by the dashed line [89F2].

For Fig. 545 see p. 351.

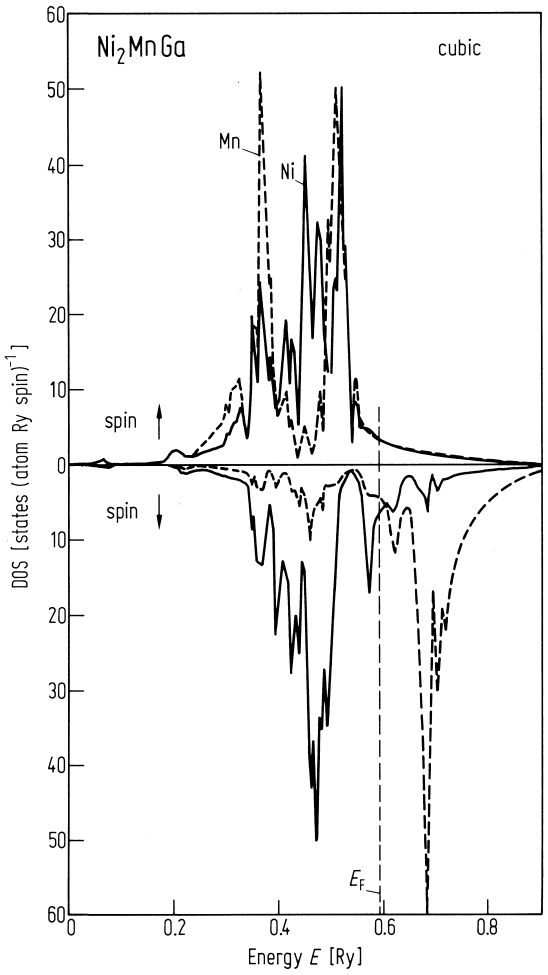

Fig. 546. DOS curves of ferromagnetic Ni_2MnGa, cubic structure. The Fermi level is indicated by the vertical broken line. The solid and broken curves show the DOS for d bands of Ni and Mn respectively and the DOS curves for up-spin electrons are shown in the upper side and those for down-spin in the lower side [89F2].

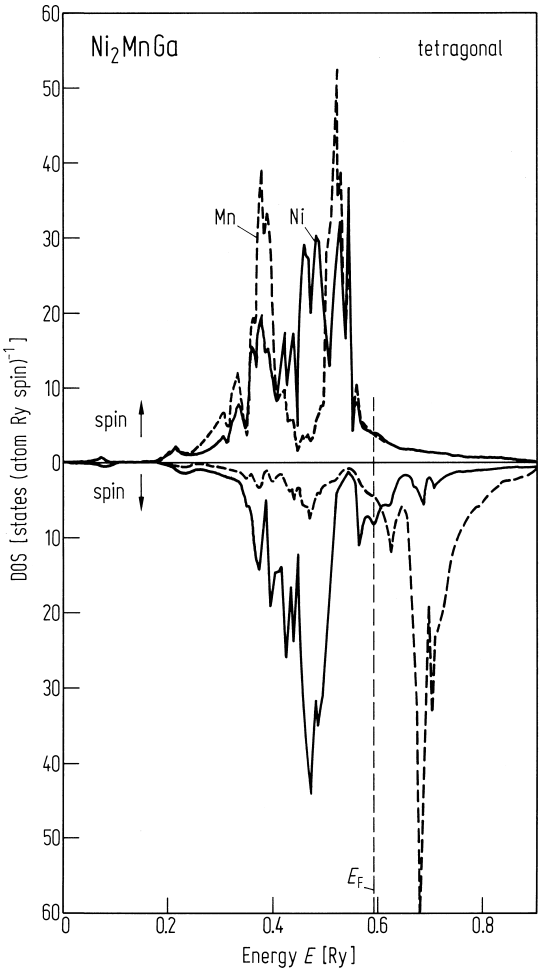

Fig. 547. DOS curves of ferromagnetic Ni_2MnGa, tetragonal structure. The Fermi level is indicated by the vertical broken line. The solid and broken curves show the DOS for d bands of Ni and Mn respectively and the DOS curves for up-spin electrons are shown in the upper side and those for down-spin in the lower side [89F2].

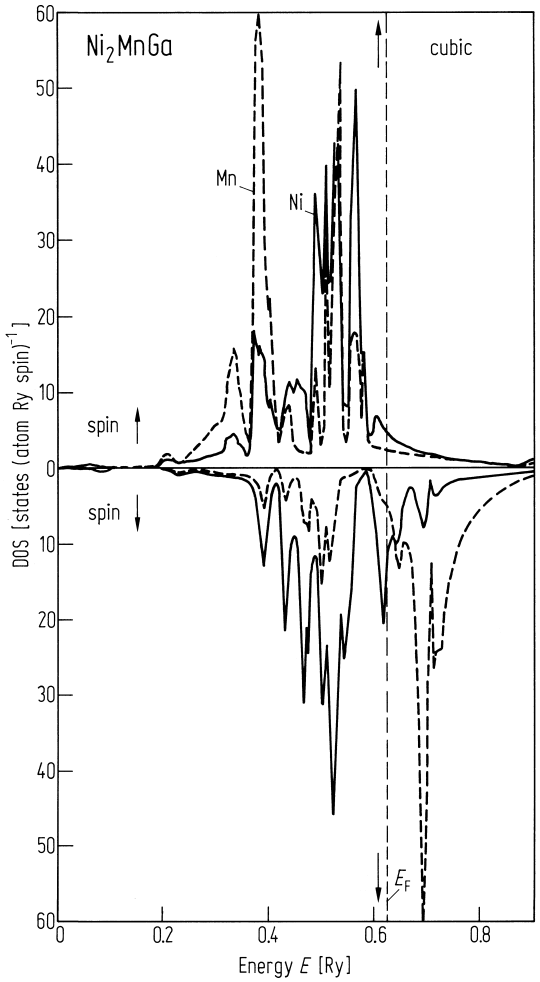

Fig. 548. Artificial DOS curves of cubic Ni_2MnGa. The Fermi level is indicated by the vertical broken line. Arrows indicate the Fermi level of $Ni_2(Mn_{1-x}V_x)Ga$ at x = 0.1. The DOS curves of d-bands of Ni and Mn are shown by the solid and broken curves respectively [89F2].

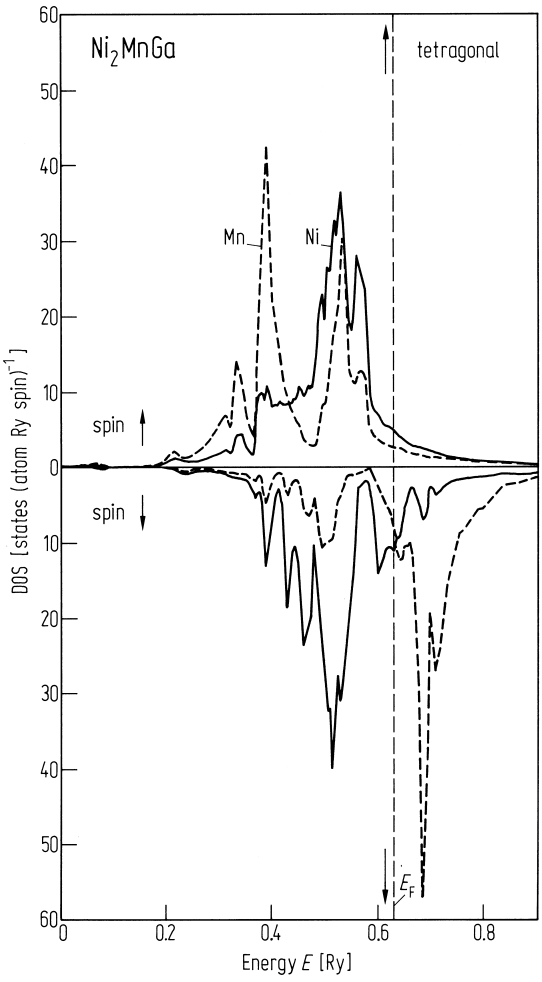

Fig. 549. Artificial DOS curves of tetragonal Ni_2MnGa. The Fermi level is indicated by the vertical broken line. Arrows indicate the Fermi level of $Ni_2(Mn_{1-x}V_x)Ga$ at x = 0.1. The DOS curves of d-bands of Ni and Mn are shown by the solid and broken curves respectively [89F2].

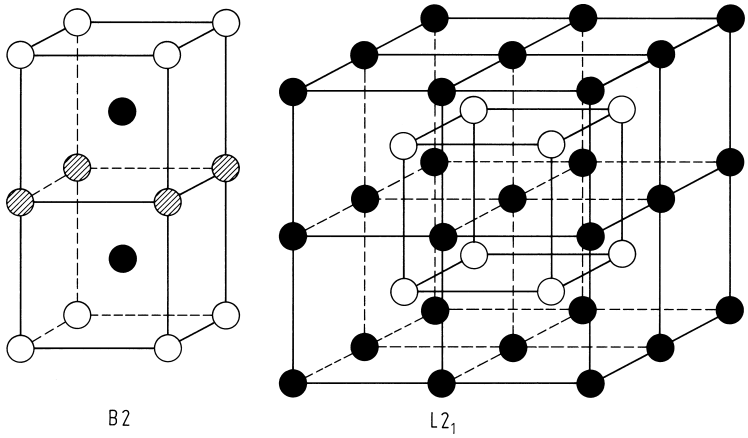

Fig. 550. Unit cell of the $L2_1$ and B_2 structures [92L1].

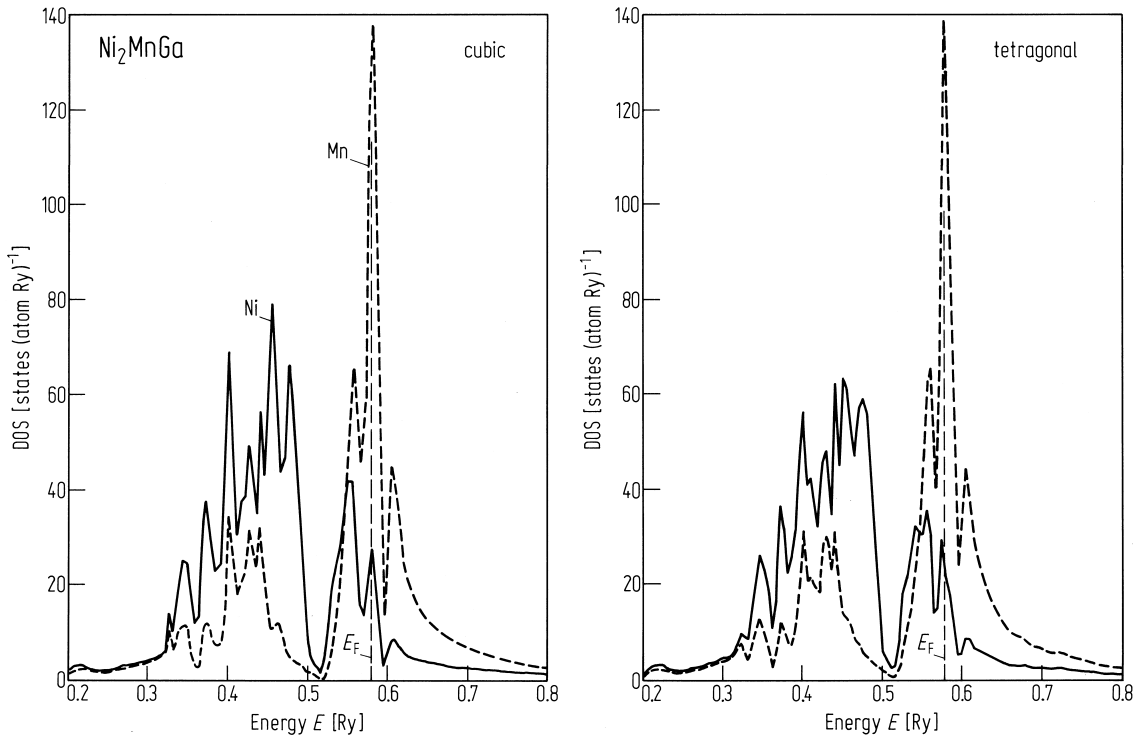

Fig. 545. DOS curves of paramagnetic Ni_2MnGa. The Fermi level is indicated by the vertical broken line. The DOS curves of d bands of Ni and Mn are shown by the solid and broken curves respectively. The DOS for the cubic structure is shown on the left, that of tetragonal one on the right [89F2].

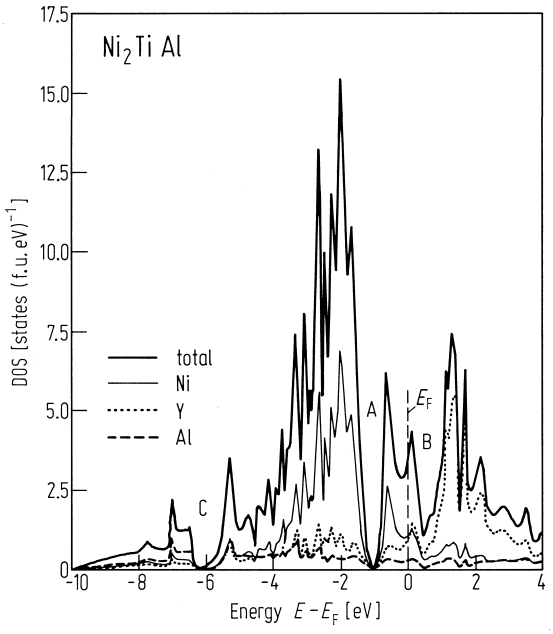

Fig. 551. Total and projected site DOS of the $L2_1$ Heusler phase Ni_2YAl, Y = Ti. The thick solid line denotes a total DOS, and the thin solid, dotted and broken lines represent the site DOS of the Ni, Y and Al respectively (DOS in states/ eV atom). A, B, C denote the valleys in the density of states, with A and C being so deep that they create semiconductor-like gaps in the DOS [92L1].

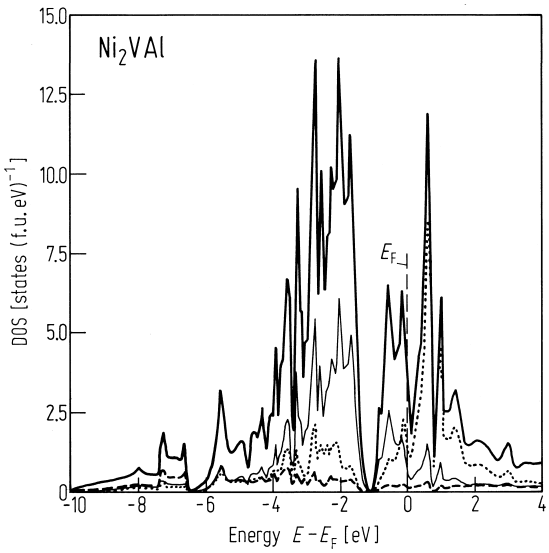

Fig. 552. Total and projected site DOS of the $L2_1$ Heusler phase Ni_2YAl, Y = V. For notation of the curves see Fig. 551 [92L1].

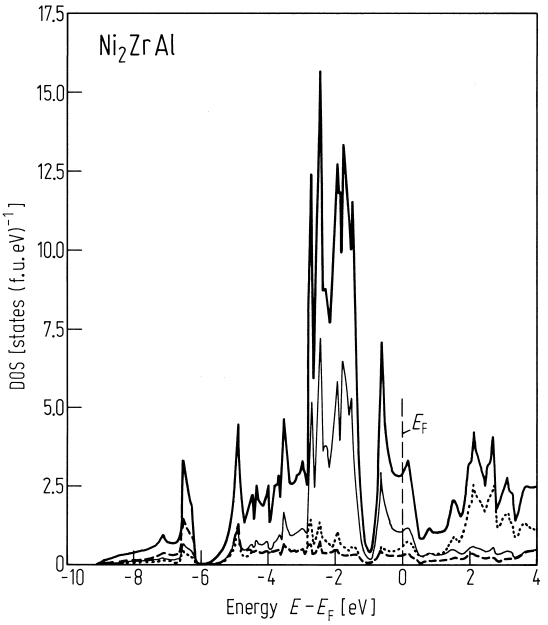

Fig. 553. Total and projected site DOS of the $L2_1$ Heusler phase Ni_2YAl, Y = Zr. For notation of the curves see Fig. 551 [92L1].

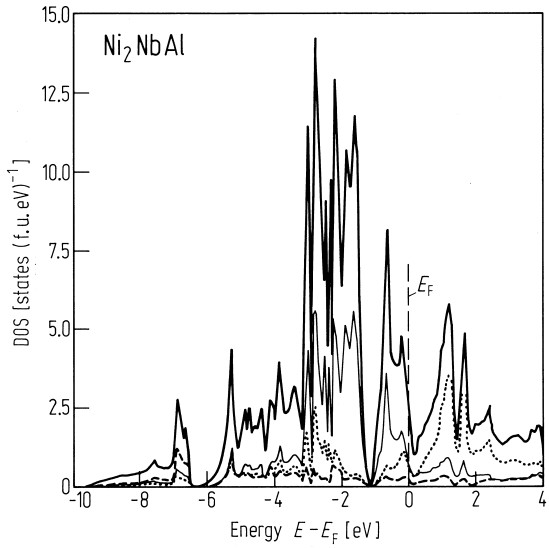

Fig. 554. Total and projected site DOS of the $L2_1$ Heusler phase Ni_2YAl, Y = Nb. For notation of the curves see Fig. 551 [92L1].

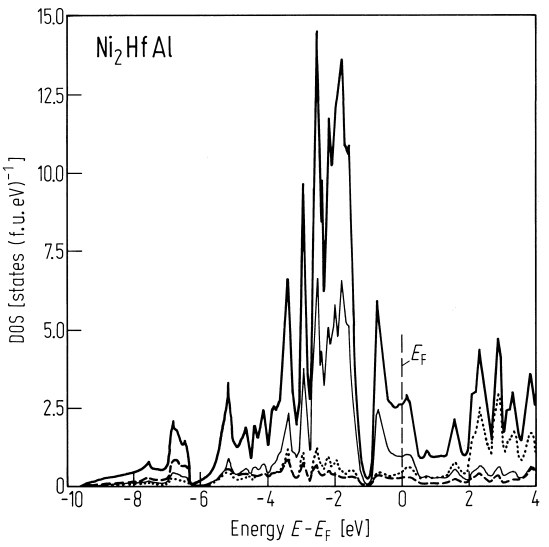

Fig. 555. Total and projected site DOS of the $L2_1$ Heusler phase Ni_2YAl, Y = Hf. For notation of the curves see Fig. 551 [92L1].

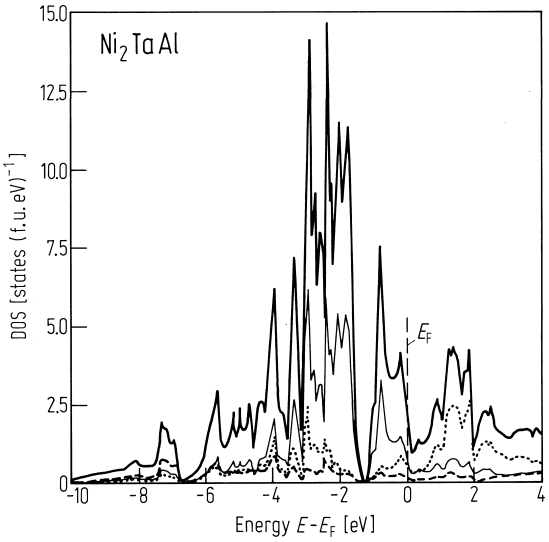

Fig. 556. Total and projected site DOS of the $L2_1$ Heusler phase Ni_2YAl, Y = Ta. For notation of the curves see Fig. 551 [92L1].

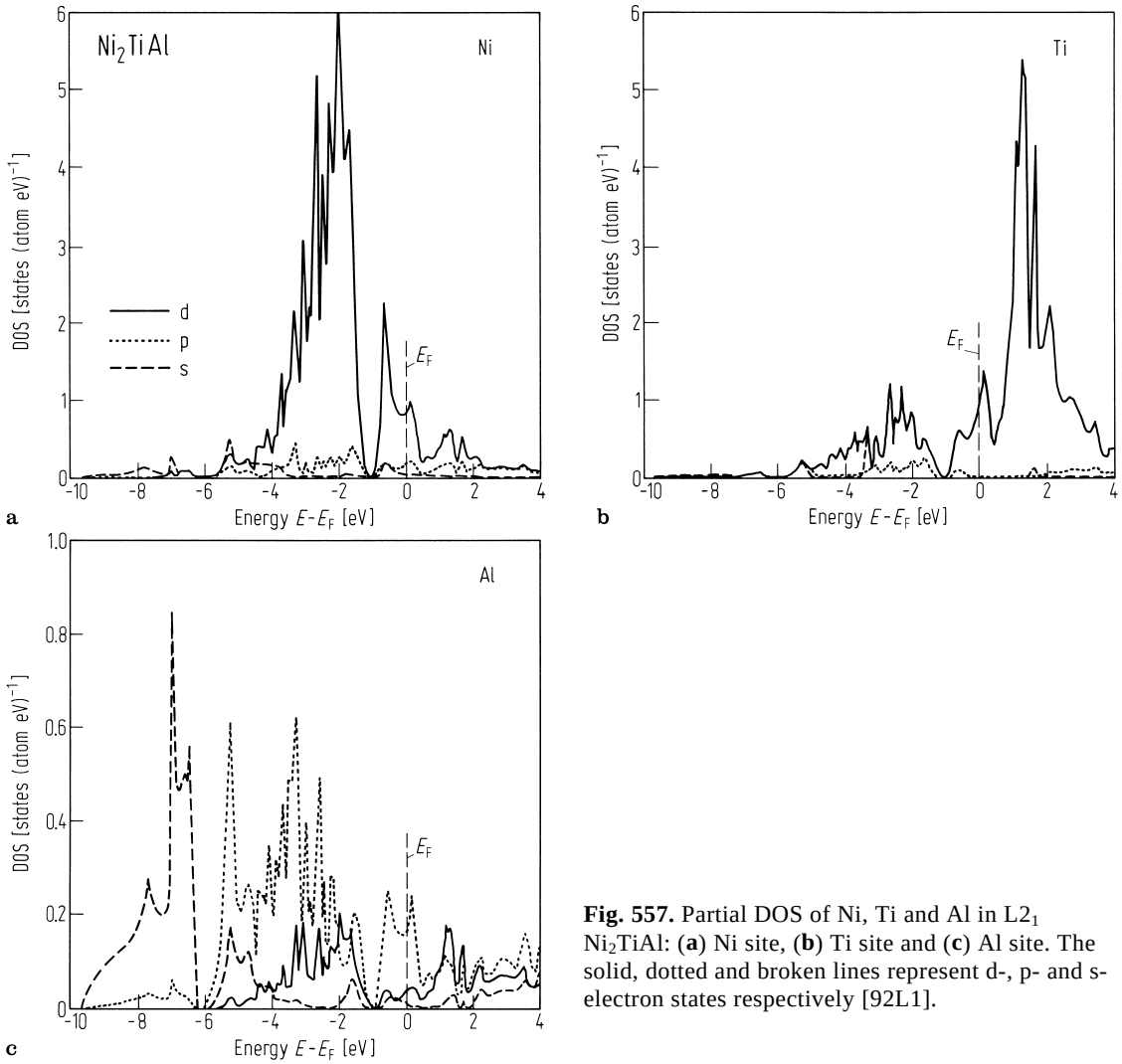

Fig. 557. Partial DOS of Ni, Ti and Al in $L2_1$ Ni_2TiAl: (**a**) Ni site, (**b**) Ti site and (**c**) Al site. The solid, dotted and broken lines represent d-, p- and s-electron states respectively [92L1].

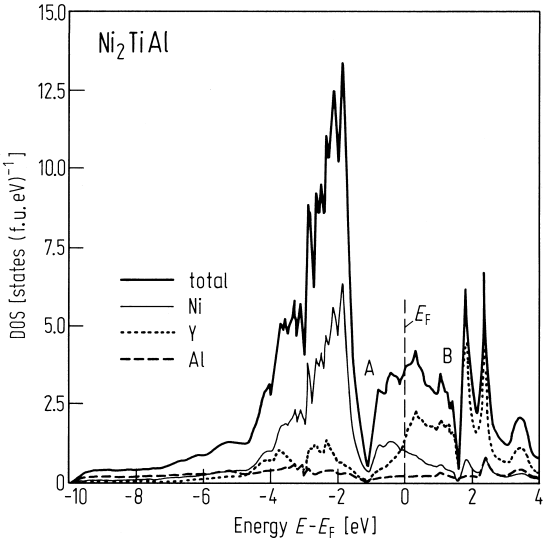

Fig. 558. Total and projected site DOS for the B2 phase Ni_2YAl, Y = Ti. The thick solid line denotes the total DOS, and the thin solid, dotted and broken lines represent the site DOS (in states /eV atom) of Ni, Y and Al respectively. A and B denote the valleys in the density of states [92L1].

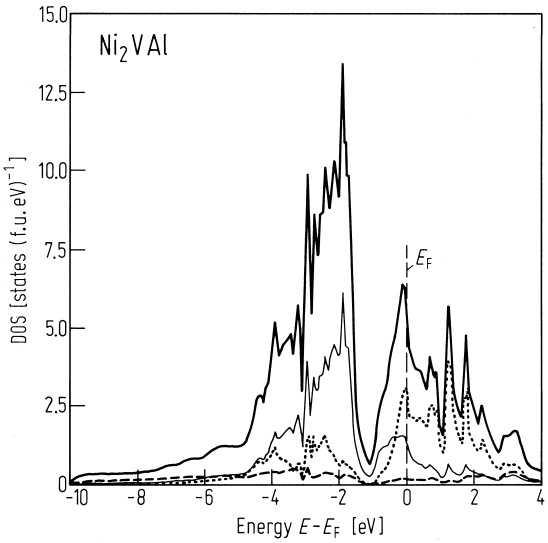

Fig. 559. Total and projected site DOS for the B2 phase Ni_2YAl, Y = V. For notation of the curves see Fig. 558 [92L1].

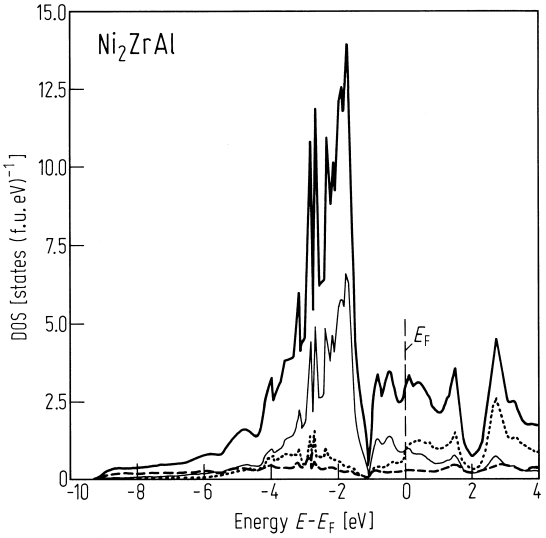

Fig. 560. Total and projected site DOS for the B2 phase Ni_2YAl, Y = Zr. For notation of the curves see Fig. 558 [92L1].

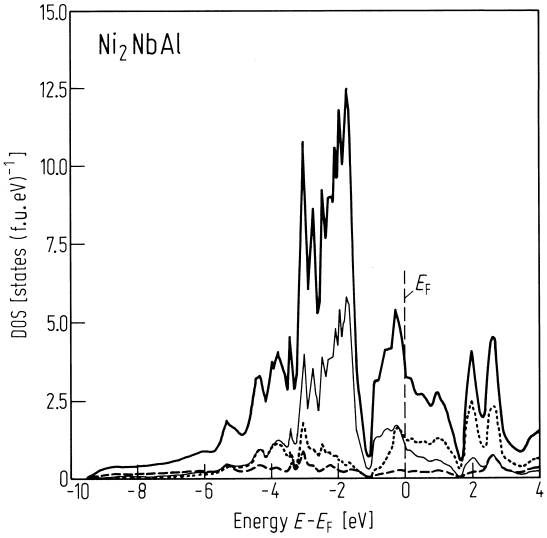

Fig. 561. Total and projected site DOS for the B2 phase Ni_2YAl, Y = Nb. For notation of the curves see Fig. 558 [92L1].

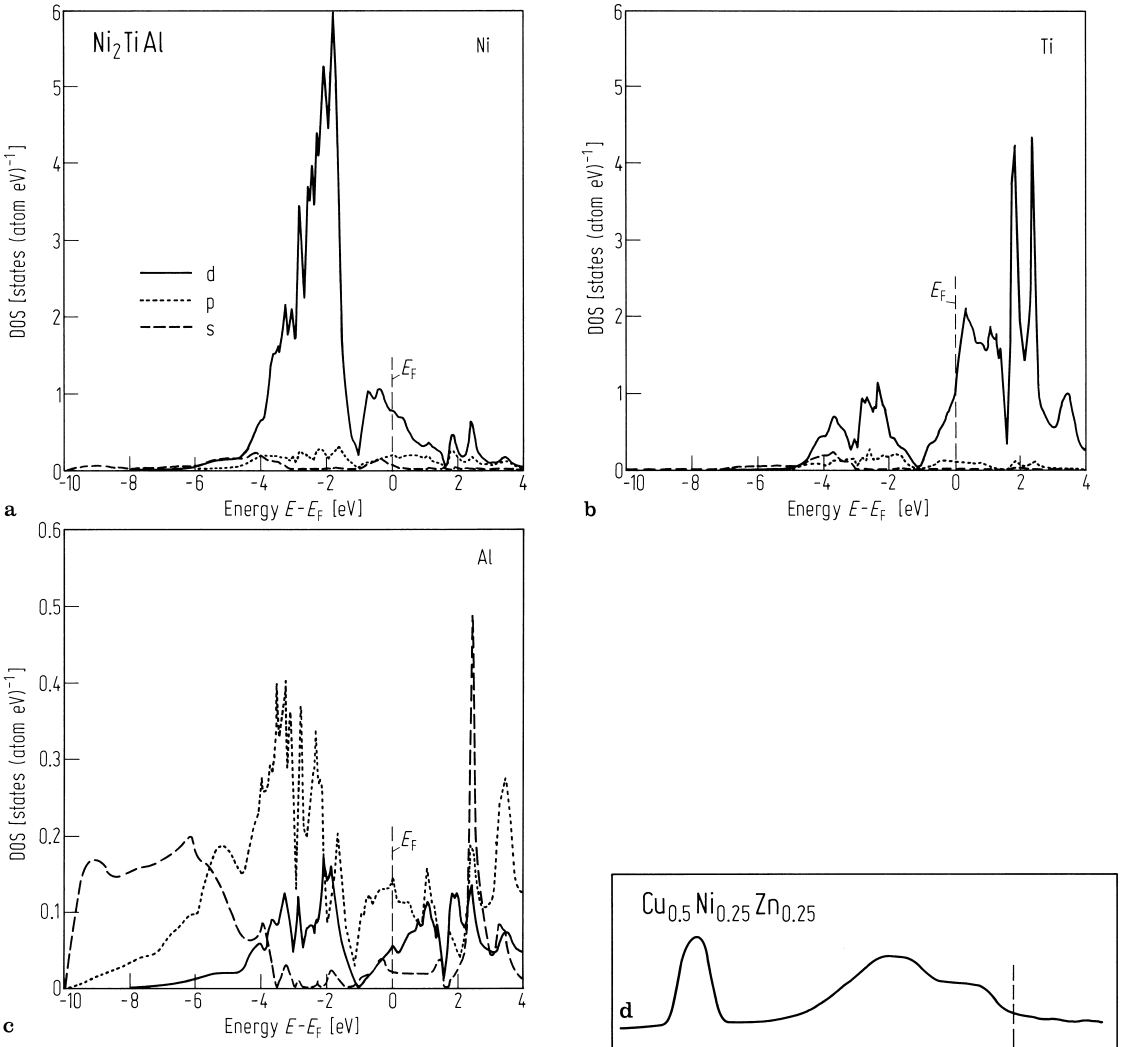

Fig. 562. Partial DOS of Ni, Ti and Al in B2-like Ni_2TiAl. (**a**) Ni site, (**b**) Ti site and (**c**) Al site. The solid, dotted and broken lines represent d-, p- and s-electron states respectively [92L1].

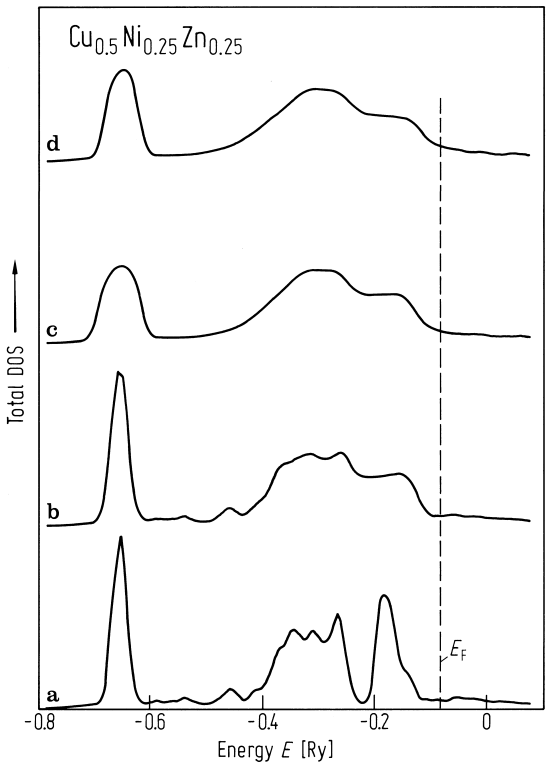

Fig. 564. Total densities of states for (**a**) the ordered Heusler-type alloy $Cu_{0.5}Ni_{0.25}Zn_{0.25}$, (**b**) the alloy with the local atomic ordering, (**c**) the completely disordered alloy without lattice relaxations, and (**d**) the completely disordered alloy with lattice relaxations. The Fermi levels are indicated by long vertical lines [91K1].

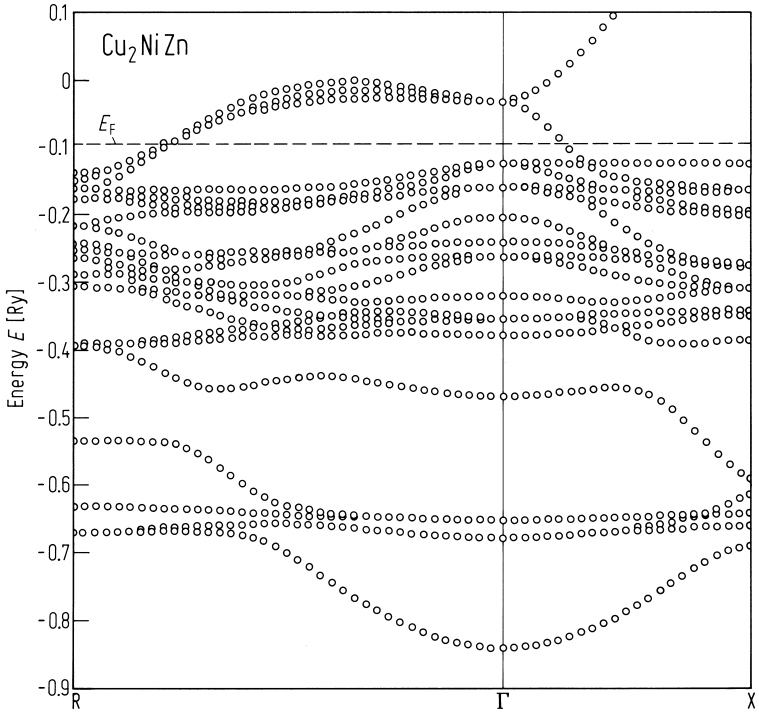

Fig. 563. Scalar relativistic bands of the ordered Heusler alloy Cu_2NiZn along the line R-Γ-X in the simple cubic Brillouin zone. The horizontal line denotes the position of the Fermi level [91K1].

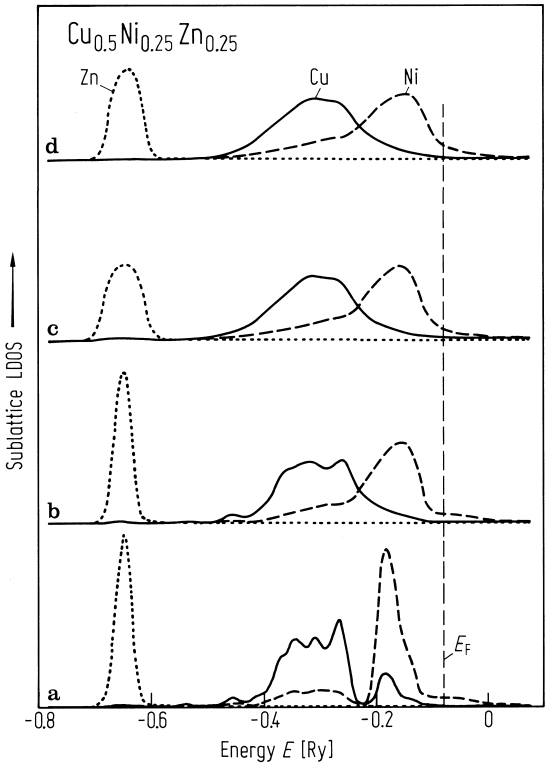

Fig. 565. $Cu_{0.5}Ni_{0.25}Zn_{0.25}$ as in Fig. 564 but for the local density of states on Cu atoms (solid lines), Ni atoms (dashed lines), and Zn atoms (dotted lines). The local density of states are not concentration weighted. The local density of states on Zn atoms have been multiplied by a factor of 0.5 to prevent the corresponding (dotted) curves from shooting beyond the allotted frames [91K1].

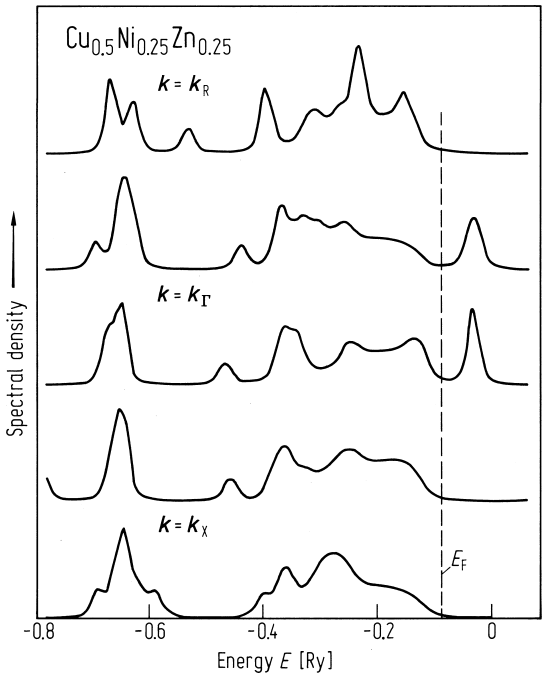

Fig. 566. Bloch spectral densities along the R-Γ-X in the simple cubic Brillouin zone for $Cu_{0.5}Ni_{0.25}Zn_{0.25}$ with local atomic ordering (case (**b**) in Figures 564 and 565). The position of the Fermi level is indicated by the long vertical lines [91K1].

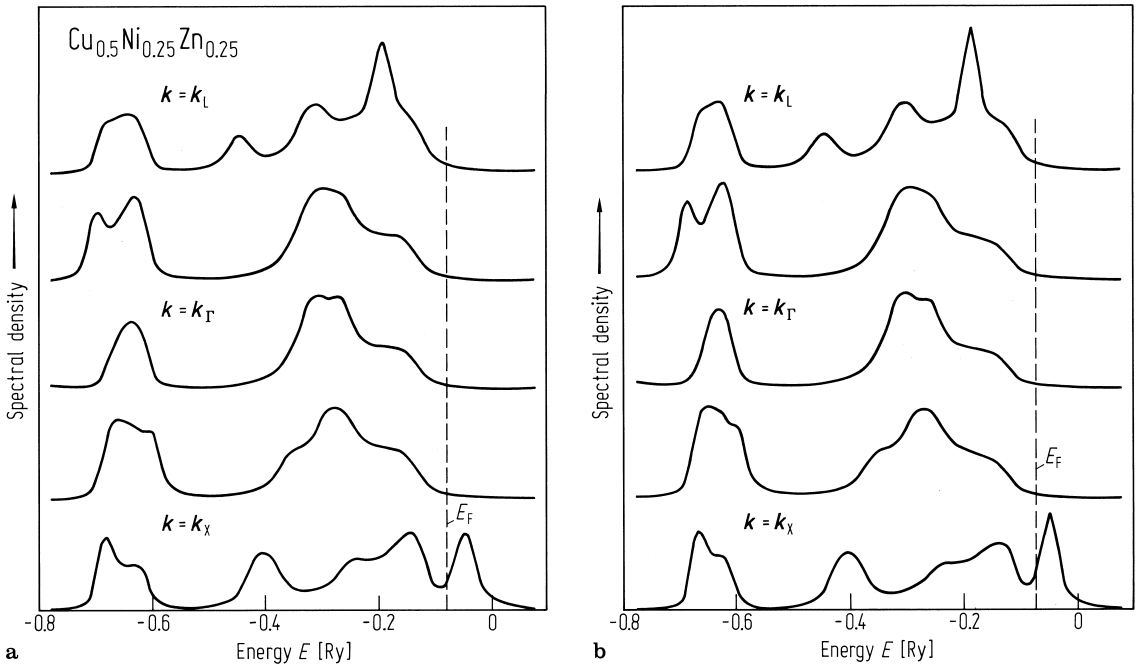

Fig. 567. Bloch spectral densities along the lines L-Γ-X in the fcc Brillouin zone for the completely disordered alloy $Cu_{0.5}Ni_{0.25}Zn_{0.25}$ (**a**) without lattice relaxations and (**b**) with lattice relaxations. The long vertical lines indicate the Fermi levels [91K1].